EIS and IRT for Evaluating Lithium Batteries

Subjects: Engineering, Electrical & Electronic

Contributor: Ximena Carolina Acaro Chacón , Stefano Laureti , Marco Ricci , Gregorio Cappuccino

During lithium-ion batteries (LIBs) ordinary operation, safety concerns are related to the possibility of overheating and, in extreme cases, to the risk of fire or explosion. Hence, it is crucial to implement proper safety measures in the design, manufacturing, and in the second life of LIBs, through a proper design of thermal management systems or short circuit protection. Regarding their durability, LIBs can face degradation over time due to repeated charge–discharge cycles. This might affect their charge retention capacity and their lifespan. Hence, ongoing research is being conducted to improve these aspects through advancements in materials, electrode design, and battery management systems. LIB development focuses on improving their efficiency by using environmentally friendly materials. The non-destructive testing (NDT) of LIBs can be classified into several categories. The commonly accepted taxonomy is based on their underlying physical principle of measurement, e.g., electromagnetic waves, thermal waves, mechanical waves, etc.

non-destructive testing | non-destructive evaluation | lithium battery | experimental setup | state-of-health | second life usage | electrochemical impedance spectroscopy | infrared thermography | X-ray

2. Electromechanical Impedance Spectroscopy (EIS)

Electrochemical impedance spectroscopy (EIS) is based on the measurement of the battery impedance over a range of frequency values. Impedance is a measure of the opposition of a battery over the electrical current flow as a function of the input frequency, i.e., it is the AC counterpart of the resistance in a DC circuit. EIS is used to estimate several battery parameters that are related to the SOC, such as internal resistance, capacity, and time constant [1][2]. The remarkable aspect of EIS is the ability to provide insight into both the intrinsic characteristics and the surface properties of a system, leveraging parallels to circuit elements.

Figure 1 shows a basic experimental setup for the EIS test, which makes use of an impedance analyzer connected to the electrodes and excites them via an AC voltage/current input in a range of frequency values. In general, a four-electrode cell is used, but in practical applications on commercial cells, a two-electrode configuration is the only one that can be employed, although this leads to a less-precise control of the potential across the electrochemical interface of the cell [3][4].

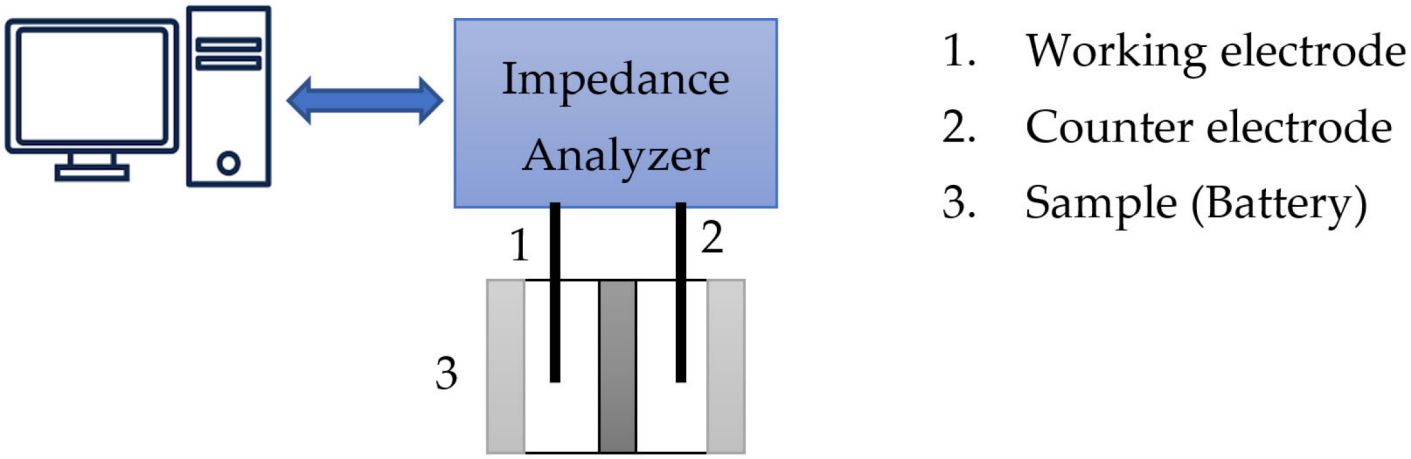

Figure 1. Typical representation of electrochemical impedance spectroscopy (EIS) measurements of a LIB presented in a test setup.

According to the systems theory, the LIB is here considered to be a black box and the response to AC potential or current signals is retrieved over a range of frequencies. The value of the impedance is computed from the mentioned system's output over a set of frequency values, thus resulting in a spectroscopy method. Practically speaking, this means that the diffusion coefficients, kinetic parameters, and electrolyte resistance of the LIB can be retrieved using a single measurement. The impedance is calculated according to Equations (1) and (2). Equation (3) shows how the imaginary (reactance) and real (resistance) parts of the impedance can be used to compute the phase angle, from which meaningful parameters can be inferred. The values of both the resistance and the reactance can also be plotted against each other, i.e., the so-called Nyquist plot, and this can provide further information about the LIB.

In Equations (1)–(3), Vt stands for the potential as a function of time t, It is the current, $\hat{V}$ the amplitude of voltage, $\hat{I}$ the amplitude of current, $\varnothing$ is the phase shift, Zo is the magnitude of impedance, and Z' and Z'' the reactance and resistance, respectively.

As a final remark, note also that galvanostatic EIS is frequently applied to LIBs as well [5].

$$Z = \frac{V_t}{I_1} = \frac{\hat{V}\sin(wt)}{\hat{I}\sin(wt+\emptyset)} = Z_0\frac{\sin(wt)}{\sin(wt+\emptyset)} \quad (1)$$

$$Z_0 = \sqrt{(Z')^2 + (Z'')^2} \quad (2)$$

$$\tan(\emptyset) = \frac{Z'}{Z''} \quad (3)$$

It must be stressed that EIS data can be used to infer and/or select suitable equivalent circuit models (ECMs) to switch between the mentioned black box approach with a large number of free parameters to smaller, more interpretable, yet controllable, ones. The choice of a given ECM model to describe the behavior of LIBs is not an easy task and it depends on several factors, such as the dynamic range, working conditions, and the battery type (LiPo, $LiFePO_4$, etc.), as they have different electrochemical characteristics and impedance behaviors, performance at low and high frequencies, the electrochemical components such as electrodes, electrolytes, and separators, the specific application, and eventually, the accuracy to be reached [6][7]. In the framework of battery research and development, highly accurate modelling is sought, while in other processes such as control applications, a simplified representation may be sufficient. To establish accurate circuit models, a range of proper electrical components, e.g., capacitors, resistors, inductors, and diodes, representing the overall system should be used.

It is important to note that there is no ECM that can be adapted to all types of batteries, though it can be customized depending on the characteristics and specific applications [8][9][10]. As a matter of fact, according to the properties of the electrochemical cell, a customized circuit model can be created by incorporating or excluding electrical components from an existing one. This is just a snapshot, but it gives an insight into the importance of choosing appropriate ECMs and the difficulties related to such a decision. Once an ECM has been selected and an EIS conducted, it is possible to evaluate fundamental properties that are crucial for understanding and optimizing the performance of batteries through data modelling and parameter analysis.

Related Works

In [5][11], the authors provided an overview of strategies for battery temperature estimation based on EIS. These strategies involve direct phase shift and intercept frequency measurements. To establish the effectiveness of these EIS-based techniques, the authors ran a comparative analysis with other existing apparatus and methods such as temperature sensors, equivalent circuits, and numerical models. Their findings demonstrated that the EIS response profiles are faster in detecting temperature peaks occurring within the LIB compared to conventional temperature measurements.

Furthermore, a study [12] presented a review of how to construct a physically sound circuit model according to the characteristics of the battery system. By establishing a precise circuit model and constructing a uniform cell system to perform an EIS analysis, crucial information about each LIB's component can be obtained. EIS can separate and quantify the *Rb*, *RSEI*, R_{ct} and *W* by a single experiment, and this can be used to analyze the battery characteristics regarding the state of charge (SOC), temperature, and SOH. EIS can be used to identify highly sensitive parameters (Ohmic resistance, capacitance of the SEI film, charge conduction resistance, and others) that are related to a change in the SOH.

In [13], the authors proposed a time-domain EIS measurement technique followed by an equivalent circuit model interpretation. One of the difficulties in modelling is the choice of initial values, which often makes numerical convergence unachievable if these are wrongly set. The authors of [7] proposed a method to determine and optimize suitable parameters for battery analysis. The method was tested by applying it to two different kinds of LIBs: a lithium iron phosphate (LFP) battery and a lithium cobalt oxide (LCO) one. The proposed method combines several criteria to select a set of suitable values for each parameter, and then employs a quantitative criterion, the so-called Kramers–Kronig relations, to select an optimal parameter value among them. The proposed algorithm is computationally light, and it has been demonstrated that it helps provide meaningful information when used to interpret experimental EIS data.

Recent works make use of ECM and machine learning, including artificial (ANNs) or recurrent neural networks. In particular, machine learning methods have been utilized to enhance the precision and effectiveness of EIS data, enabling the analysis of large datasets of measurements and the creation of predictive models for electrochemical systems. A model for high energy density that uses impedance spectroscopy measurements to monitor the SOH with ANNs has been proposed in [14], and it is based on an equivalent circuit approach. This phenomena is considered important and occurs inside the cell and the subsequent non-linearity of some parameters. In [15], two models for SOH estimation were proposed: one uses a convolution neural network (CNN) to process EIS data, while the other employs a bidirectional long short-term memory (BiLSTM) model for serial regression prediction. Additionally, the authors of [16] established the mapping relationship between health features and SOH using a BP neural network algorithm.

Table 1 provides a summary regarding the primary studies focusing on the prediction of SOC and SOH using EIS. As discussed above, these studies encompass the utilization of two main methodologies: ECMs and machine learning techniques (MLTs). In the case of ECMs, it is possible to obtain important values from each component in a lithium-ion cell via a single experiment. If a circuit model is established with due care and a uniform cell system is constructed to perform an EIS analysis, crucial information about each component of the LIB can be obtained. The experimental measurements can be carried out easily regardless of the battery's state and size. The MLT approach is instead useful when the underlying physical models are not known and/or when the analyzed LIB's systems are rather complex. The effectiveness of MLTs depends largely on the quality of the data, on the appropriate choice of algorithm, and on the correct interpretation of the results. As shown in **Table 1**, several studies try to combine both the approaches, i.e., the ECMs and MLTs, to speed up the process and reduce the amount of error, leading to more robust and interpretable results with respect to their standalone usage.

Table 1. Studies on predicting SOH based on EIS.

Refs.	Parameter	Error (%)	Battery Type	Experimental Setup	Characteristics
[5]	T	<1	Pouch	Abin Battery Cycler Potentiostat: Gamry Interface 5000P, Pennsylvania, USA MZTC Arbin climate-controlled	LCO Li-polymer. Real-time estimator. Online acquisition of impedance ECM was used to interpret and

Refs.	Parameter	Error (%)	Battery Type	Experimental Setup	Characteristics
					analyze the impedance data at each temperature. Sensitivity to temperature. Low sensitivity to SOC and SOH. ECM: $R_o - (CPE_1//(R_{ct} - W))$
[14]	SOH	<1	Pouch	Electrochemical Workstation (unreported)	Electrode: $LiMnNiCoO_2$ $LiPF_6$ Recurrent neural networks (RNNs). Model for high energy density dedicated to EVs. ECM: $R_1 - (R_{2(SOC)}//CPE_1) - CPE_2 - E_{(SOC)}$
[15]	SOH	~5	Coin	Electrochemical Workstation(unreported)	Eunicell LR2032. Five different ECMs. Data-driven algorithm with CNN. ECM and IPSO-CNN-BiLSTM ECM: $R_{ohm} - Ls - (R_{SEI}//C_{PE1}) - (R_{ct}//C_{PE2})$
[16]	RUL	<1	Coin	Electrochemical Workstation (unreported)	Eunicell LR2032. $LiCoO_2$/graphit Real-time battery forecasting system. Gaussian process model and ML. Over 20,000 EIS spectra of commercial Li-ion batteries, with different states of health.
[17]	SOH	3.73–8.66	Pouch	Potentiostat: Gamry Series G300 Keithley 2420 Source Meter Opto-isolated relay board (Devantech RLY816)	LiPO Performance under load. Used parameters of ECM to reproduce the discharge curves. ECM: $R_{ohm} - L - (CPE_1//R_{ct1}) - (CPE_2//R_{ct2}) - W$
[18]	SOH	2	Cylindrical	Electrochemical Workstation(unreported)	Commercial Li-ion cells ECM 10 kHz–1 MHz at different SOCs, SOHs, and temperatures. ECM based on the physics of the system. A transmission line model: $(L//R_o) - R_c - [C_g//(C_1//(R_1 + Z_{d1}) - R_e - C_2//(R_2 + Z_{d2}))]$

Refs.	Parameter	Error (%)	Battery Type	Experimental Setup	Characteristics
[19]	SOH	1.29–4	Cylindrical	Boling BLC-300 (battery test incubator) Solartron analytical 1470E NEWARE BTS-5V6A	Battery model: 18650. Anode: Graphite. Cathode: $LiNi_{0.5}C_{0.2}Mn_{0.3}O_2$ Model-based method. ECM: $R_\Omega - Ls - (CPE_1//R_{SEI}) - (CPE_2//R_{ct})$
[20]	SOH	<1.36	Coin	Electrochemical Workstation(unreported)	Eunicell LR2032. Elman NN and cuckoo search (CS-Elman). No building of a circuit model, no consideration of the complex electrochemical reaction.
[13]	SOH	<10 before 240 cycles	Cylindrical	Signal generator V/I converter circuit module (DAQ of NI)	UR14500P Type: $LiCoO_2$. TDIS (time-domain EIS) based on FFT SOH is established by using BPNN (back-propagation NN) algorithm. ECM: $[(C_{dln}//Z_{FDn}) - R_{film}]//C_{film} - R_o - (C_{dlp}//Z_{FDp})$

statistical
al. These
verity and
pends on
ity of the
ne system
ed data is
o keep in
mind the limitations of any approach.

In conclusion, EIS is a method that in combination with data-driven techniques can achieve high accuracy and it is commonly used for battery characterization and monitoring in the automotive and energy storage industries. It can be used to evaluate the electrochemical properties, SOC, SOH, and battery performance. EIS helps in identifying degradation mechanisms, tracking aging effects, and to optimize battery management strategies. Based on the various studies and works analyzed here, this NDT technique is a cost-effective solution in various industrial applications. The cost to arrange an EIS setup can vary depending on the specific requirements, the desired accuracy, and the frequency range of interest, but is in general relatively low.

3. Infrared Thermography (IRT)

IRT is extensively used for quality control and process monitoring in a plethora of industrial applications [21]. Infrared cameras rely on the principle of heat transfer through radiation, and they contain a focal plane array composed of elements capable of capturing the infrared spectrum emitted by the surfaces of the objects. The impinging radiation is converted into digital data, which are then displayed as an image, and are visualized within the visible spectrum in false color [22][23][24]. Some cameras are calibrated using radiometric references to accurately record and display measurements in specific units. These cameras are endowed with various sensor types and pixel resolutions in order to capture specific infrared wavebands at the needed level of spatial detail.

For the analysis of LIBs, active thermography systems are increasingly used, in particular the pulsed IRT by exploiting flash lamps. In pulsed IRT, the excitation source is the flashlight. The surface of the battery is exposed to a brief, intense heat pulse produced by the flashlight, see **Figure 2**. If the LIB's internal structure is flawless and relatively homogeneous, the heat diffuses at the same speed throughout a section of it, thus resulting in a homogenous distribution of the LIB surface temperature. A flaw such as a delamination, a vacancy, or the inclusion of a foreign body, affects the heat diffusion locally, resulting in temporal variations or discrepancies of the surface temperature that can be captured by the IR camera. A computer, equipped with real-time image signal processing and analysis, grabs a time sequence of thermal signals (one for each pixel of the camera sensor), revealing the propagation of thermal energy from the surface to the interior of the target and vice versa.

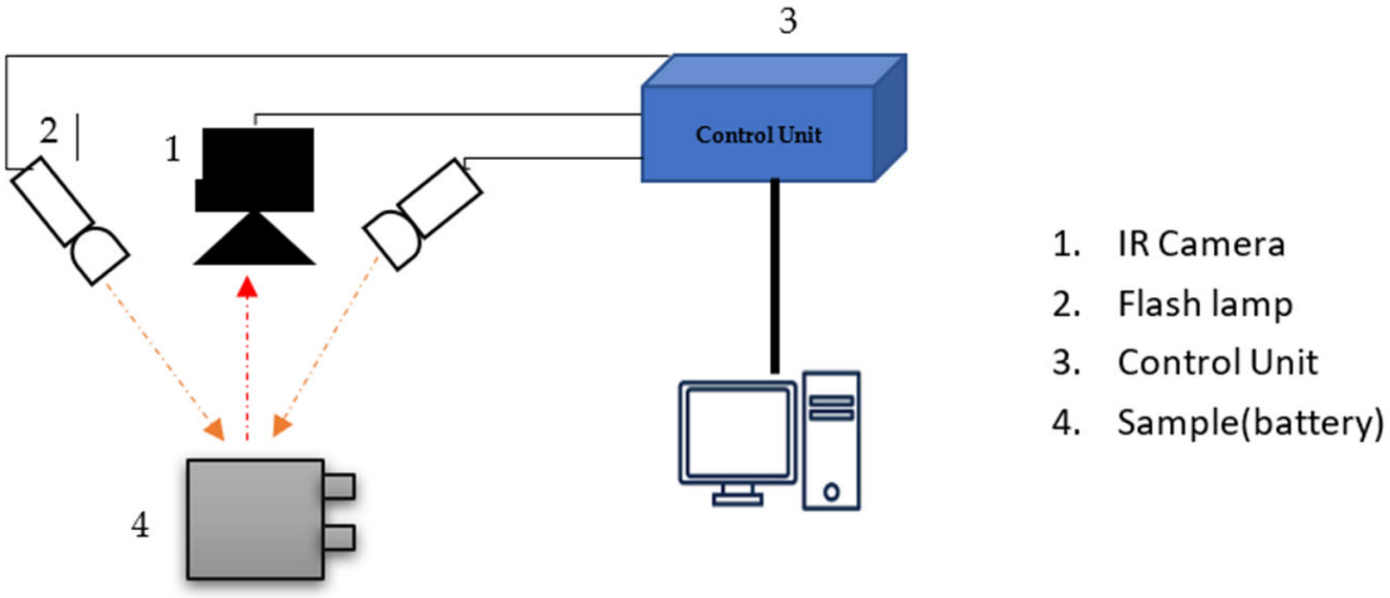

Figure 2. Basic test setup of infrared thermography in reflection mode.

On the other hand, in the passive IRT approach, the heat source is the battery itself. Heat losses within a battery occur from multiple sources, including the entropy change resulting from electrochemical reactions and the Joule's effect, or ohmic heating, caused by current flow across internal resistances and overpotential, see Equation (4). In certain electrochemical combinations, additional electrical energy losses occur, leading to heat generation, for e.g., when attempting to overcharge a fully charged cell.

The first term in Equation (4), represents the heat generation attributed to the reversible entropy change due to the electrochemical reactions within the cell. The second term, accounts for the heat generation resulting from irreversible effects such as ohmic heating and other factors within the cell [25]. Based on these terms and on the discussion above, if the thermal performance of battery pack is not taken into consideration, the rising temperature can cause severe damages to it.

$$q = \left(-I \left[T \left(\frac{dE}{dT} \right) \right] \right) + I \left(E - V \right) \quad (4)$$

In Equation (4), q is the heat generation, I the current, T the temperature, the term dE/dT is the temperature coefficient, E the open-circuit potential, and V the cell potential.

Related Works

In [26], an experimental assessment of a commercial $LiFePO_4$ battery's thermal and electrical performance is reported. The paper highlights that thermal management of LIBs is a key problem for electric mobility applications, where batteries are subject to severe operating conditions. The comparison between passive IRT and thermocouple probe measurements showed that the surface temperature was not uniform along the height of the battery, with a greater warming up in its upper zone. In addition to the thermal analysis, the authors also reported an electrical characterization of the LIB, including the cell potential, open circuit potential, and entropic heat coefficient vis à vis the SOC, which were experimentally measured. The obtained experimental data were used to evaluate a simplified heat generation term that is widely employed in numerical approaches.

In [27], the authors discusses the use of pulsed IRT for the inspection of composite material batteries. The article proposes a method for detecting defects in such material using an advanced combination of pulsed thermography and image processing techniques.

In order to foresee the internal heat generation of a lithium-ion pouch cell, the combined use of a lumped capacitance model and thermography is proposed in [28], using a polyimide film heater positioned in front of an IR camera. A series of experiments were carried out to confirm the new method. This method is used to foresee the rate of heat generation in a lithium iron phosphate cell at various discharge rates.

In works [29][30], IRT and thermocouple measurements were used to compare the surface temperatures of lithium-ion polymer cells at various rates of discharge. The experimental measurement aimed at tracking the evolution of the surface temperature of commercial bag cells. The IR images revealed the spatial distribution of the surface temperature, and it was found that the location of the hot spots varies as a function of both the geometrical and material properties of the cell, and according to the type/amount of load applied to the cells.

Various research studies related to thermal analysis and evaluation of different cells are reported in **Table 2**. The different experimental approaches, methods, and results obtained have been considered in the reported taxonomy. The amount of research performed demonstrates the significance of thermal evaluation in understanding the behavior and performance of batteries. The use of IRT and thermocouple measurements to assess the surface temperature and thermal power estimation seems to be a common approach across the studies. These methods offer valuable insights into the thermal behavior and potential issues of batteries. For instance, the use of pulsed IRT combined with image processing techniques shows promise for defect detection in composite/multi-layer

materials. However, when performing pulsed IRT it is important to consider factors such as the difficulty of achieving uniform heating across the battery's surface, as well as thermal conductivity limitations. Additionally, a new non-contact steady-state method for measuring thermal conductivity and thermal contact resistance has been reported [31], providing an alternative approach to evaluating the thermal properties of the battery cell's components.

Table 2. Studies on predicting state of LIB based on IRT.

Refs.	Parameter	Error (%)	Battery Type	Experimental Setup	Characteristics
[26]	H-generation	<0.1	Cylindrical	(RMX-4125) programmable power supply (RMX-4005)-DC electronic load NI 6289-data acquisition FLIR SC3000 IR camera thermocouple	Positive and negative electrodes $LiFePO_4$ and LiC_6. Electrolyte $LiPF_6$. IT and thermocouple probe Increase in the thermal power when the battery is subjected to higher discharge currents. Efficiency decreased with higher C-rates. It describes a heat generation model.
[27]	Thermal abuse	1	Pouch	Li-Polymer battery Infrared camera-FLUKE	$LiFePO_4$ The security problem lies in thermal control, including the heat-generation and the internal and external heat transfer.
[28]	H-generation	2.6	Pouch	polyimide film heater FLIR A320-calorimeter	$LiFePO_4$ Mathematical model (Biot number, LCM) Lumped capacitance model (LCM) and thermography. Not to be applied where the C-rate is 2C or lower.
[29]	Surface temperature	<10%	Pouch LCO	FLIR E6 thermal imaging camera, thermocouples, humidity sensor black cardboard Applent AT4808 Handheld Multi-channel Temperature Meter	It compares the surface temperature at different discharging rates by infrared thermography and thermocouple measurements. Temperature rises rapidly at higher discharge rates.
[30]	Surface temperature	<1	Pouch NMC, LCO, LPF	NMC-based, LFP, LTO ACT 0550 (80 channels) battery tester (PEC®). NTC 5K thermistor	Evolution of surface temperature. Non-uniformity of the surface temperature.

Refs.	Parameter	Error (%)	Battery Type	Experimental Setup	Characteristics
				Ti25 thermal imager (FLUKE®)	
[31]	Thermal conductivity	12.2	Cilindrical 18650	Coating (XFNANO) laser (MDL-III-808-2W, CNI) Camera (MAG32MINI, Magnity).	Negative electrode: $Li_4Ti_5O_{12}$ Non-contact steady-state method. Equivalent thermal circuit.
[32] [33]	Defects	1	Coin	FLIR SC-8200 Carl Zeiss Merlin SEM Bruker Nano GmbH using an XFlash 5030 detector Hitachi S3400 SEM	Positive electrode: $LiNi_{0.5}Mn_{0.3}Co_{0.2}O_2$ Different plausible defects (agglomeration, blisters, pinholes, metal particle contamination, and non-uniform coating).
[34]	Detection of gas pockets	1	Pouch	PL-565068 infrared camera (FPA InSb FLIRSC5000MB) Potentiostat-IviumStat Current probe-Tektronix A622. Digital acquisition unit-USB 6363 Software-Altair	It demonstrates the effectiveness in the detection of gas pockets formed during cell aging.
[35]	Thermal	1	pouch	ThermaCam-SC640 Fluke 867B multimeter TENMA 72-10505 power supply block TENMA 72-13200 electronic load.	Thermal behavior at different charging and discharging modes.
[36]	H-generation	1	Pouch	Environmental chamber-(Tenney T10c) IR-camera (T650sc, FLIR) T-type thermocoupleSA1-T infrared (IRW-4C, FLIR) Battery tester-BT2000, Arbin Instruments.	Cathode: $LiNi_{0.6}Co_{0.2}Mn_{0.2}O_2$, anode: graphite. Suggesting uniform heating. Hotspot is detected at the activation terminal for improvement of SHLB design. SHLB (self-heating of LIB).
[37]	Cycle Life (RUL)	<10%	pouch	MLX90621-infrared sensor array SUNKEE module ACS712 current sensor. N103-voltage sensors	Combination of infrared thermography and supervised learning techniques. Surface temperature profiles as the input nodes for ANN and SVM models. ANN could estimate the current

about its accurate inspected nt thermal ed by the thermal camera. IRT can also be used to identify the introduction of contaminating particles, the formation of defects during electrode creation, or to identify holes and a lack of bulk material. The accuracy and sensitivity of the technology depends on the camera quality, calibration, and environmental considerations. While there are a

Refs.	Parameter	Error (%)	Battery Type	Experimental Setup	Characteristics
					cycle under 10 min of testing time.

e desired
ost of the
termining
gas pockets and abnormal heat-generation within the battery.

References

1. Meddings, N.; Heinrich, M.; Overney, F.; Lee, J.-S.; Ruiz, V.; Napolitano, E.; Seitz, S.; Hinds, G.; Raccichini, R.; Gaberscek, M. Application of electrochemical impedance spectroscopy to commercial Li-ion cells: A review. J. Power Sources 2020, 480, 228742.
2. Padha, B.; Verma, S.; Mahajan, P.; Arya, S. Electrochemical Impedance Spectroscopy (EIS) Performance Analysis and Challenges in Fuel Cell Applications. J. Electrochem. Sci. Technol. 2022, 13, 167–176.
3. Lazanas, A.C.; Prodromidis, M.I. Electrochemical Impedance Spectroscopy—A Tutorial. ACS Meas. Sci. Au 2023, 3, 162–193.
4. Hogg, B.-I.; Waldmann, T.; Wohlfahrt-Mehrens, M. 4-Electrode Full Cells for Operando Li+ Activity Measurements and Prevention of Li Deposition in Li-Ion Cells. J. Electrochem. Soc. 2020, 167, 090525.
5. Carthy, K.; Gullapalli, H.; Kennedy, T. Real-time internal temperature estimation of commercial Li-ion batteries using online impedance measurements. J. Power Sources 2022, 519, 230786.
6. Zheng, Y.; Shi, Z.; Guo, D.; Dai, H.; Han, X. A simplification of the time-domain equivalent circuit model for lithium-ion batteries based on low-frequency electrochemical impedance spectra. J. Power Sources 2021, 489, 229505.
7. Fernández Pulido, Y.; Blanco, C.; Anseán, D.; García, V.M.; Ferrero, F.; Valledor, M. Determination of suitable parameters for battery analysis by Electrochemical Impedance Spectroscopy. Measurement 2017, 106, 1–11.
8. Andre, D.; Meiler, M.; Steiner, K.; Walz, H.; Soczka-Guth, T.; Sauer, D.U. Characterization of high-power lithium-ion batteries by electrochemical impedance spectroscopy. II: Modelling. J. Power Sources 2011, 196, 5349–5356.
9. Habte, B.T.; Jiang, F. Effect of microstructure morphology on Li-ion battery graphite anode performance: Electrochemical impedance spectroscopy modeling and analysis. Solid State Ionics 2018, 314, 81–91.
10. Westerhoff, U.; Kurbach, K.; Lienesch, F.; Kurrat, M. Analysis of Lithium-Ion Battery Models Based on Electrochemical Impedance Spectroscopy. Energy Technol. 2016, 4, 1620–1630.

11. Li, D.; Wang, L.; Duan, C.; Li, Q.; Wang, K. Temperature prediction of lithium-ion batteries based on electrochemical impedance spectrum: A review. Int. J. Energy Res. 2022, 46, 10372–10388.
12. Choi, W.; Shin, H.C.; Kim, J.M.; Choi, J.Y.; Yoon, W.S. Modeling and applications of electrochemical impedance spectroscopy (Eis) for lithium-ion batteries. J. Electrochem. Sci. Technol. 2020, 11, 1–13.
13. Lyu, C.; Zhang, T.; Luo, W.; Wei, G.; Ma, B.; Wang, L. SOH Estimation of Lithium-ion Batteries Based on Fast Time Domain Impedance Spectroscopy. In Proceedings of the 2019 14th IEEE Conference on Industrial Electronics and Applications (ICIEA), Xi'an, China, 19–21 June 2019; pp. 2142–2147.
14. Eddahech, A.; Briat, O.; Bertrand, N.; Delétage, J.-Y.; Vinassa, J.-M. Behavior and state-of-health monitoring of Li-ion batteries using impedance spectroscopy and recurrent neural networks. Int. J. Electr. Power Energy Syst. 2012, 42, 487–494.
15. Li, D.; Yang, D.; Li, L.; Wang, L.; Wang, K. Electrochemical Impedance Spectroscopy Based on the State of Health Estimation for Lithium-Ion Batteries. Energies 2022, 15, 6665.
16. Zhang, Y.; Tang, Q.; Zhang, Y.; Wang, J.; Stimming, U.; Lee, A.A. Identifying degradation patterns of lithium ion batteries from impedance spectroscopy using machine learning. Nat. Commun. 2020, 11, 1706.
17. Galeotti, M.; Ciná, L.; Giammanco, C.; Cordiner, S. Performance analysis and SOH (state of health) evaluation of lithium polymer batteries through electrochemic. Energy 2015, 89, 678–686.
18. Ezpeleta, I.; Freire, L.; Mateo-Mateo, C.; Nóvoa, X.R.; Pintos, A.; Valverde-Pérez, S. Characterisation of Commercial Li-Ion Batteries Using Electrochemical Impedance Spectroscopy. ChemistrySelect 2022, 7, e202104464.
19. Zhang, Q.; Huang, C.G.; Li, H.; Feng, G.; Peng, W. Electrochemical Impedance Spectroscopy Based State-of-Health Estimation for Lithium-Ion Battery Considering Temperature and State-of-Charge Effect. IEEE Trans. Transp. Electrif. 2022, 8, 4633–4645.
20. Chang, C.; Wang, S.; Jiang, J.; Gao, Y.; Jiang, Y.; Liao, L. Lithium-Ion Battery State of Health Estimation Based on Electrochemical Impedance Spectroscopy and Cuckoo Search Algorithm Optimized Elman Neural Network. J. Electrochem. Energy Convers. Storage 2022, 19, 030912.
21. Alfredo Osornio-Rios, R.; Antonino-Daviu, J.A.; De Jesus Romero-Troncoso, R. Recent industrial applications of infrared thermography: A review. IEEE Trans. Ind. Inf. 2019, 15, 615–625.
22. Hou, F.; Zhang, Y.; Zhou, Y.; Zhang, M.; Lv, B.; Wu, J. Review on Infrared Imaging Technology. Sustainability 2022, 14, 11161.
23. Balakrishnan, G.K.; Yaw, C.T.; Koh, S.P.; Abedin, T.; Raj, A.A.; Tiong, S.K.; Chen, C.P. A Review of Infrared Thermography for Condition-Based Monitoring in Electrical Energy: Applications and

Recommendations. Energies 2022, 15, 6000.

24. Usamentiaga, R.; Venegas, P.; Guerediaga, J.; Vega, L.; Molleda, J.; Bulnes, F. Infrared Thermography for Temperature Measurement and Non-Destructive Testing. Sensors 2014, 14, 12305–12348.
25. Pesaran, A.A.; Burch, S.D. Thermal Performance of EV and HEV Battery Modules and Packs Prepared under FWP HV71; National Renewable Energy Laboratory: Golden, CO, USA, 1997; p. 997.
26. Giammichele, L.; D'Alessandro, V.; Falone, M.; Ricci, R. Thermal behaviour assessment and electrical characterisation of a cylindrical Lithium-ion battery using infrared thermography. Appl. Thermal Eng. 2022, 205, 117974.
27. Wang, Z.-j.; Li, Z.-q.; Liu, Q. Infrared thermography non-destructive evaluation of lithium-ion battery. In International Symposium on Photoelectronic Detection and Imaging 2011: Advances in Infrared Imaging and Applications; SPIE: Beijing, China, 2011; pp. 1237–1244.
28. Bazinsky, S.J.; Wang, X. Predicting heat generation in a lithium-ion pouch cell through thermography and the lumped capacitance model. J. Power Sorces 2016, 305, 97–105.
29. Rani, M.F.H.; Razlan, Z.M.; Shahriman, A.B.; Ibrahim, Z.; Wan, W.K. Comparative study of surface temperature of lithium-ion polymer cells at different discharging rates by infrared thermography and thermocouple. Int. J. Heat Mass Transf. 2020, 153, 119595.
30. Goutam, S.; Timmermans, J.M.; Omar, N.; Van den Bossche, P.; Van Mierlo, J. Comparative study of surface temperature behavior of commercial li-ion pouch cells of different chemistries and capacities by infrared thermography. Energies 2015, 8, 8175–8192.
31. Liu, Y.; Xu, S.; Wang, Y.; Dong, H. Non-contact Steady-State Thermal Characterization of Lithium-Ion Battery Plates Using Infrared Thermography. Int. J. Thermophys. 2022, 43, 131.
32. Mohanty, D.; Hockaday, E.; Hensley, D.K.; Daniel, C.; Wood, I.D. Effect of electrode manufacturing defects on electrochemical performance of lithium-ion batteries. J. Power Sources 2016, 312, 70–79.
33. Mohanty, D.; Li, J.; Born, R.; Maxey, L.C.; Dinwiddie, R.B.; Daniel, C.; Wood, D.L. Non-destructive evaluation of slot-die-coated lithium secondary battery electrodes by in-line laser caliper and IR thermography methods. Anal. Methods 2014, 6, 674–683.
34. Robinson, J.B.; Engebretsen, E.; Finegan, D.P.; Darr, J.; Hinds, G.; Shearing, P.R.; Brett, D.J.L. Detection of internal defects in lithium-ion batteries using lock-in thermography. ECS Electrochem. Lett. 2015, 4, A106–A109.
35. Stoynova, A.; Bonev, B.; Rizanov, S. Thermographic Study of Thermal Processes during Battery Charging and Discharging. In Proceedings of the 2021 44th International Spring Seminar on

Electronics Technology (ISSE), Bautzen, Germany, 5–9 May 2021.

36. Zhang, G.; Tian, H.; Ge, S.; Marple, D.; Sun, F.; Wang, C.-Y. Visualization of self-heating of an all climate battery by infrared thermography. J. Power Sources 2018, 376, 111–116.
37. Zhou, X.; Hsieh, S.-J.; Peng, B.; Hsieh, D. Cycle life estimation of lithium-ion polymer batteries using artificial neural network and support vector. Microelectron. Reabil. 2017, 79, 48–58.